Preparation of Ultrathin Supported Solid Electrolyte Membranes for Oxygen Separation

Andreas Ziehfreund and Wilhelm F. Maier*

Max-Planck-Institut für Kohlenforschung, Kaiser-Wilhelm-Platz 1, 45470 Mülheim an der Ruhr, Germany

Received March 13, 1996. Revised Manuscript Received July 18, 1996[⊗]

Physical vapor deposition methods, e.g., reactive electron beam evaporation and reactive rf sputtering, were used to prepare ultrathin (<1 μm) layers of solid electrolytes with oxygen ionic conductivity. For stabilization commercially available mesoporous support membranes with pore diameters of 20 nm were used. Partially defective electrolyte layers were additionally modified by a special sol−gel dipcoating technique to reduce defect concentration. Resulting membranes were nearly defect-free with overall relative permeabilities less than 0.5%, in the case of sputtered membranes 0.1%. Gas separation experiments performed with stabilized zirconia electrolyte membranes, prepared by thermal evaporation with sol−gel modification, showed that the transport mechanism is dominated by Knudsen diffusion. This is due to high intrinsic microporosity of the polycrystalline film material, confirmed by gas adsorption measurements. In contrast bismuth molybdate and lead−magnesium oxide membranes, made by rf sputtering, showed some specific oxygen enrichment at higher temperatures (300 °C) that could not be explained exclusively by Knudsen diffusion. This could possibly be due to selective oxygen separation through the electrolyte layer by ways of oxygen ionic conduction.

Introduction

Oxygen ion conducting solid electrolytes are materials capable of absorbing oxygen from the gas phase and transporting it as oxide ions by an electrochemical defect mechanism. Potential applications for solid electrolyte membranes are gas separations, power generation (solid oxide fuel cells[1]), oxygen sensors (automotive pollution control[2]), and catalysis (catalytic membrane reactors,[3] electrocatalysis[4]). Selective oxidation by membrane catalysis is of particular interest in chemical research. Connections between catalytic activity and electrochemical transport properties of certain oxide catalysts are obvious but still not well understood.[5,6] Oxygen transport across an oxide ion conducting membrane is partially limited by bulk−ionic and electronic conductivity of the membrane material and surface exchange rates of the oxygen.

Major problems of present oxygen selective membranes are the high operating temperature (>600 °C) normally required for oxygen ion conductivity and the rather low permeability. For practical separation applications significantly lower operating temperatures and higher permeabilities are needed. The need for low-temperature oxygen transporting materials was recently outlined as one of the major opportunities in future materials research.[7] To advance the field, improved membranes or oxygen-transport materials have to be developed. Concepts for the optimization of oxygen selective membranes can be formulated as follows:

Minimal Membrane Thickness. According to the theory of electrochemical transport by Wagner,[8] eq 1 gives the oxygen flux across the bulk zone of a solid electrolyte membrane, driven by a chemical potential gradient:

$$J_{O_2} = \frac{1}{4^2F^2l}\int_{\mu_{I,O_2}}^{\mu_{II,O_2}} t_{ion}t_{el}\sigma \, d\mu_{O_2} \qquad (1)$$

F is the Faraday constant, l is the membrane thickness, t_{ion} and t_{el} are the ionic and electronic transport numbers, and σ is the total conductivity of the membrane material. Since the oxygen flux is reversely proportional to membrane thickness, the development of extremely thin membranes should improve the situation. Since defect formation can be caused by microscopic dust particles, microorganisms, or chemical rearrangement processes, we estimate the lower limit of thickness for such membranes to be around 0.1 μm. Therefore a membrane thickness between 0.1 and 1 μm should be a realistic target, which if prepared free of defects should provide the required stability.

Use of Mixed Conducting Oxides. According to eq 1 the flux of a pure ionic conductor (t_{ion} > 0.99) is limited by the intrinsic electrical conductivity of the material, unless there is no external bridging of the membrane surfaces. Mixed (ionic and electric) conduc-

[⊗] Abstract published in *Advance ACS Abstracts,* October 1, 1996.

(1) Minh, N. Q. *J. Am. Ceram. Soc.* **1993**, *76*, 563.
(2) Logothetis, E. M. In: *Advances in Ceramics*; The American Ceramic Society: Columbus, OH, 1981; Vol. 3, p 388.
(3) Saracco, G.; Specchia, V. *Catal. Rev.−Sci. Eng.* **1994**, *36*, 305.
(4) Metcalfe, I. S. *Catal. Today* **1994**, *20*, 283.
(5) Gellings, P. J.; Bouwmeester, H. J. M. *Catal. Today* **1992**, *12*, 1.
(6) Zhang, Z.; Verykios, X. E.; Baerns, M. *Catal. Rev.−Sci. Eng.* **1994**, *36*, 507.
(7) Armor, J. N. *Chem. Mater.* **1994**, *6*, 730.
(8) Heyne, L. Electrochemistry of mixed ionic-electronic conductors. In: *Solid electrolytes*; Geller, S., Ed.; Springer-Verlag: Berlin; *Top. Appl. Phys.* **1977**, *21*, 169.

S0897-4756(96)00195-0 CCC: $12.00

tivity within the same material allows discharge of the oxygen anions at the surface by an internal short circuit and avoids the buildup of a blocking surface layer.

Catalytic Surface Activation of Oxygen. Below a certain membrane thickness, oxygen exchange at the membrane surface will become the rate-limiting step for permeation. Addition of an oxygen-activating catalyst such as platinum may lower the activation barrier for surface oxygen exchange. This may result in a lower effective transport temperature thus enlarging the oxygen flux.

Introduction of Internal Surface Area by Means of Porosity. Porosity increases the accessible membrane surface area and may be a trivial method for enhancing the oxygen flux. The advantage of increased flux has to be counterbalanced by the potential loss in oxygen selectivity due to pore-transport mechanisms. Enhancements in oxygen currents by 2 orders in magnitude have been predicted by Abeles et al. for porous oxide electrodes relative to nonporous electrodes.[9]

Most publications on oxygen semipermeable ceramic membranes are based on bulk materials in the thickness range 0.5−1.5 mm.[10−15] The preparation of thin membranes is still an unsolved problem with conventional methods. Electrochemical vapor deposition[16] is the most commonly used technique for the preparation of thin solid electrolyte films, namely, stabilized zirconia, in the range <50 μm. Recently a combination of electrochemical and chemical vapor deposition has been reported for the manufacturing of very thin layers of solid electrolytes (0.5−1.5 μm).[17] In this report we describe, to our knowledge for the first time, the preparation of ultrathin (<1 μm) ceramic membranes made from solid oxide electrolytes by methods of physical vapor deposition, i.e., electron beam evaporation and rf sputtering, partially modified by a sol−gel dipcoating procedure.

Well-known examples for oxygen ion conductors are the so-called stabilized zirconias, in which the cubic structure of the ionic conducting high-temperature modification of zirconia is stabilized at room temperature by the addition of alkaline earth or rare earth oxides.[18] Other examples for oxygen-conducting solid electrolytes include doped ceria, thoria, or bismuth oxide. Bismuth-containing compounds are especially promising, because of their remarkably high oxygen conductivity at relatively low temperatures (<600 °C).[19]

Table 1 summarizes the composition of the oxygen ion conducting materials selected as membrane materials in this study. Doping of stabilized zirconia with n-type semiconducting oxides, in our case titania and ceria (compounds 2 and 3, Table 1) is supposed to lead to solid electrolytes with enlarged electronic conductivities at low O_2 partial pressure.[20,21] Bismuth molybdate Bi_2MoO_6 and a mixed lead− magnesium oxide PbO−MgO, both of which are catalysts for selective oxidation applications, were also used as membrane materials. Bismuth molybdate is known to be a very good mixed conductor with high conductivities even at low temperatures.[22] PbO−MgO is also assumed to be a low-temperature ionic, maybe mixed, conductor.[23]

Table 1. Composition of Selected Oxygen Ion Conductors

no	compound	code
1	$(ZrO_2)_{0.91}(Y_2O_3)_{0.09}$	YSZ
2	$(ZrO_2)_{0.72}(Y_2O_3)_{0.10}(TiO_2)_{0.18}$	YSZ−TiO_2
3	$(ZrO_2)_{0.72}(Y_2O_3)_{0.10}(CeO_2)_{0.18}$	YSZ−CeO_2
4	$(ZrO_2)_{0.88}(CaO)_{0.12}$	CSZ
5	$(CeO_2)_{0.89}(La_2O_3)_{0.11}$	LDC
6	$(Bi_2O_3)_{0.85}(La_2O_3)_{0.15}$	LDB

Experimental Procedure

Sample Preparation. Samples of solid electrolytes 1−5 (Table 1) were prepared from a slurry of the pure oxides in distilled water at the given composition. After drying, the samples were heated to 400 °C for 8 h, milled, and heated again to 1000 °C for 16 h. The resulting samples were then pulverized and pressed with 750 MPa to pellets 2−3 mm in thickness and 13 mm in diameter. In a final treatment step the sample pellets are heated to 1200 °C for 12 h and 1600 °C for 6 h.

LDB was prepared by coprecipitation from an aqueous acidic solution of $Bi(NO_3)_3{\cdot}5H_2O$ and $La(NO_3)_3{\cdot}6H_2O$, according to the procedure by DiCosimo et al.[24] Bismuth molybdate was prepared from a slurry of MoO_3 in an aqueous acidic solution of $Bi(NO_3)_3{\cdot}5H_2O$, analogous to the method of Batist et al.[25] PbO−MgO was made from a slurry of PbO and MgO (1:1) in dilute nitric acid followed by drying and calcination at 600 °C for 16 h.

Sputter targets of LDB, Bi_2MoO_6, and PbO−MgO were made by preparing sample pellets 2−3 mm in thickness and 50 mm in diameter using a pressure of 100 MPa. The resulting powder compacts were then heated slowly (rate 1 °C min^{-1}) to 700 °C (Bi_2MoO_6, PbO-MgO) and 740 °C (LDB) respectively for 2−3 days. During this period the target materials are mechanically stabilized and reach up to 60% of the theoretical density without too much of volume contraction, which would be disfavorable because of limitations given by the sputtering equipment used. An YSZ-10 sputter target is prepared for comparison of the different evaporation techniques with a final sintering temperature of 1000 °C.

Thin-Film and Membrane Preparation. Membranes are prepared by thin-film coating of porous substrate disks. Anopore membranes were used as support membrane for the stabilization of thin films (Al_2O_3; Whatman Science, Banbury, effective pore diameter 0.02 and 0.2 μm asymmetric pores). Pure unsupported thin-film material was prepared by coating of aluminum foil and dissolution of the metal in dilute acid.

ZrO_2- and CeO_2-containing membranes were produced by reactive electron beam evaporation at $p(O_2) = 10^{-4}$ mbar and a power of 450−825 W (high-vacuum evaporation system, Balzers BAE 250 T; electron gun, magnetically focused bent beam source, Edwards). Coating rates were in the range 20−

(9) Deng, H.; Zhou, M.; Abeles, B. *Solid State Ionics* **1994**, *74*, 75; **1995**, *80*, 213.
(10) Smith, A. W.; Meszaros, F. W.; Amata, C. D. *J. Am. Ceram. Soc.* **1966**, *49*, 240.
(11) Dou, S.; Masson, C. R.; Pacey, P. D. *J. Electrochem. Soc.* **1985**, *132*, 1843.
(12) Bouwmeester, H. J. M.; Kruidhof, H.; Burggraaf, A. J.; Gellings, P. J. *Solid State Ionics* **1992**, *53−56*, 460.
(13) Teraoka, Y.; Zhang, H.-M.; Furukawa, S.; Yamazoe, N. *Chem. Lett.* **1985**, 1743.
(14) Teraoka, Y.; Nobunaga, T.; Yamazoe, N. *Chem. Lett.* **1988**, 503.
(15) Burggraaf, A. J.; Bouwmeester, H. J. M.; Boukamp, B. A.; Uhlhorn, R. J. R.; Zaspalis, V. *Mater. Sci. Monogr.* **1991**, *75 (Sci. Ceram. Interfaces)*, 525.
(16) Isenberg, A. O. *Proc. Electrochem. Soc.* **1977**, *77−6*, 572.
(17) Cao, G. Z.; Brinkman, H. W.; Meijerink, J.; de Vries, K. J.; Burggraaf, A. J. *J. Am. Ceram. Soc.* **1993**, *76*, 2201.
(18) Etsell, T. H.; Flengas, S. N. *Chem. Rev.* **1970**, *70*, 339.
(19) Iwahara, H.; Isaka, T.; Sato, T.; Takahashi, T. *J. Solid State Chem.* **1981**, *39*, 173.
(20) Liou, S.; Worell, L. *Appl. Phys.* **1989**, *A49*, 25.
(21) Calès, B.; Baumard, J. F. *J. Electrochem. Soc.* **1984**, *131*, 2407.
(22) Boon, L.; Metselaar, R. *Mater. Sci. Monogr.* **1985**, *28A (React. Solids, Pt. A)*, 357.
(23) Omata, K.; Hashimoto, S.; Tominaga, H.; Fujimoto, K. *Appl. Catal.* **1989**, *52*, L1.
(24) DiCosimo, R.; Burrington, J. D.; Grasselli, R. K. *J. Catal.* **1986**, *102*, 234.
(25) Batist, Ph. A.; der Kinderen, A. H. W. M.; Leeuwenburgh, Y.; Metz, F. A. M. G.; Schuit, G. C. A. *J. Catal.* **1968**, *12*, 45.

100 nm min^{-1}. With a maximum coating time of 20 min a maximum thickness of 0.4−2.0 μm results. The film thickness was controlled in situ by an oscillating quartz monitor (Balzers QSG 301), calibrated externally by SEM examinations of coated substrates. Bi_2O_3-, PbO-, and ZrO_2-containing membranes were produced by reactive rf sputtering (Plasma Science, CrC-100) with a mixture of 20% O_2 in argon as sputtering gas. This method was chosen due to lower thermal stability of bismuth and lead oxide compounds. Reactive evaporation was performed at an oxygen pressure of 10^{-4} mbar.

In some cases a sol−gel dipcoating procedure is used for modification of as-coated membranes to reduce the macroscopic defect concentration of the thin-film layers. A solution of zirconium(IV)−*n*-propoxide in ethanol with addition of water and nitric acid (molar composition: 400/2/1/10 for C_2H_5OH/$Zr(n\text{-}PrO)_4$/H^+/H_2O) was used for the sol−gel process. The dipcoating procedure for preparation of microporous supported zirconia membranes has been described previously.[26]

Materials Characterization. Specific surface area and pore size distribution of thin-film materials were calculated using computer-controlled, automatic gas adsorption systems (Carlo Erba, Sorptomatic 1900; Coulter, Omnisorp 360). In the micropore region interpretation of the data followed the methods of Horvath−Kawazoe and Dubinin. The lattice structures of the solid electrolytes were determined by X-ray powder diffraction (Stoe Stadi II P). Measurements of ionic conductivity using complex impedance analysis were also performed and are described elsewhere.

For the determination of supported film structure and film defects a scanning electron microscope was used (Hitachi S-2400, 25 kV; S-2700, 30 kV; maximum resolution 4 nm). For these examinations, membranes were cut into small pieces, fixed on sample plates with conductive carbon tabs, and sputter-coated with about 10 nm of platinum.

Membrane Reactor System. For permeation and separation studies a special membrane reactor was designed (Figure 1a). The reactor allows tight mounting even of very brittle membranes material such as Anopore (d = 60 μm). The reactor is embedded in an oven with integrated Ni/Cr/Ni thermocouple and a microprocessor-controlled heating system (JUMO DICON PRS). Anopore membranes tend to break during heating because of different thermal expansion coefficients of membrane and gasket material. Therefore it was necessary to untie the reactor parts during this period and tie it just after reaching the final temperature.

The reactor is connected to a special gas flow unit using Swagelok components (Figure 1b). Gas flow through the upper chamber of the reactor is controlled by a combination of pressure controller and flow meter (Bronkhorst Hi-Tec). This setup allows gas flow control at constant pressures in the range 0.1−0.6 bar across the membrane. The permeating gas flow is monitored at the opposite side of the reactor. A quadrupole mass spectrometer (Balzers QMG 125) is used for in situ determination of gas composition at the retentate and permeate side of the membrane. A mixture of He, Ar, and O_2 (87:6.5:6.5) was used for separation experiments. The separation factor was calculated from the corrected ion current of the selected molecular ions. During every experiment the ion currents of the permeate were always compared to the ion currents of the retentate to avoid systematic errors.

Results and Discussion

X-ray Powder Diffraction. For the identification of solid electrolytes X-ray powder diffraction spectra of bulk and thin-film material were recorded.

YSZ/YSZ-TiO_2/YSZ-CeO_2/CSZ: After high-temperature treatment at 1600 °C all bulk materials showed the cubic phase of stabilized zirconia (Figure 2b). In contrast, a treatment temperature of 1000 °C, used for the preparation of zirconia sputter targets, was not high enough to produce YSZ solid solutions. In this case spectra showed a mixture of yttria and zirconia in their monoclinic phases (Figure 2a).

All evaporated films appeared to be polycrystalline. Apart from a peak broadening the thermally evaporated film shows the diffraction spectra of YSZ materials (Figure 2c). Although the sputtering target is just a physical mixture of yttria and zirconia, there is no difference between thermally evaporated and sputtered YSZ thin films. Both films consist of the cubic phase of stabilized zirconia. That indicates instant formation of the YSZ solid solution during the condensation of the sputtered/evaporated material during thin-film buildup. X-ray fluorescence spectrometric analysis of bulk and thin-film materials confirmed that there is no significant change in composition during evaporation.

LDC: The XRD spectra of highly sintered lanthana-doped ceria showed the cubic phase of ceria (cerianit). In analogy to the evaporated stabilized zirconias, the LDC films produced by electron beam evaporation are polycrystalline, showing the identical cubic phase structure of the source material.

LDB/Bi_2MoO_6/PbO−MgO: While PbO−MgO is a physical mixture of the pure oxides, Bi-based solid electrolytes are defined compounds with well-known X-ray powder diffraction spectra. The lanthana solid solution was formed in a bismuth oxide melt at 900 °C. LDB has a rhombohedral type structure, comparable to Bi_2O_3·SrO. Bi_2MoO_6 appeared to be a high-temperature modification of bismuth molybdate (γ'-Bi_2MoO_6), which is known to be formed irreversibly at 660−690 °C from a 1:1 mixture of Bi_2O_3 and MoO_3.[27] The formation of a stable γ'-Bi_2MoO_6 phase could be confirmed by DSC investigations. In contrast to zirconia- or ceria-based electrolytes all sputtered bismuth- and lead-containing film materials appeared to be X-ray amorphous.

Specific Surface Area and Pore Size Distribution. Nitrogen adsorption isotherms at 77 K showed that in contrast to all highly sintered and compact bulk electrolytes most thin film materials are microporous with high specific surface areas. This is especially the case for stabilized zirconias YSZ and CSZ, which show a narrow pore-size distribution in the micropore range and the highest specific surface area with up to 145 m^2 g^{-1} (Table 2). Adsorption measurements after treatment at higher temperatures show that the zirconia film material is of high thermal stability. The micropores remain stable up to 500 °C. Further temperature increase leads to increasing loss of micropores, but even after treatment at 1200 °C exclusively micropores with a specific surface area of about 30 m^2 g^{-1} with a broad pore-size distribution remains.

Addition of a third oxide component to the zirconia solid solutions leads to a decrease in specific surface area of the film materials, as can be seen in the case of YSZ-TiO_2 and YSZ-CeO_2. Ceria solid electrolytes of LSC-type are almost mesoporous with no distinct maximum in the pore-size distribution and a low specific surface area.

The sputtered bismuth- and lead-containing films are almost nonporous with very low surface areas. Sput-

(26) Maier, W. F.; Tilgner, I. C.; Wiedorn, M.; Ko, H. C.; Ziehfreund, A.; Sell, R. *Adv. Mater.* **1993**, *5*, 730.

(27) Shenoy, S. C.; Rao, M. S. *J. Chem. Technol. Biotechnol.* **1986**, *36*, 95.

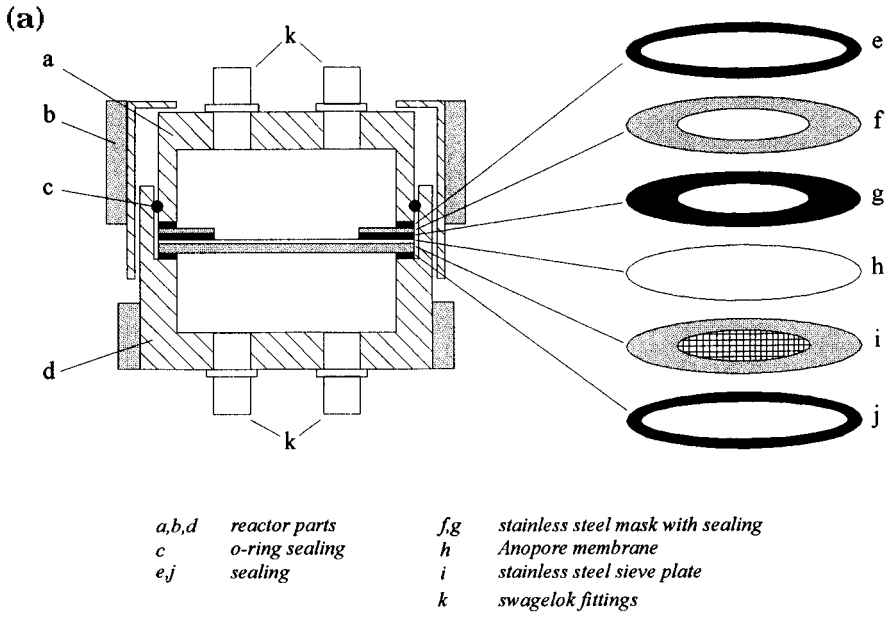

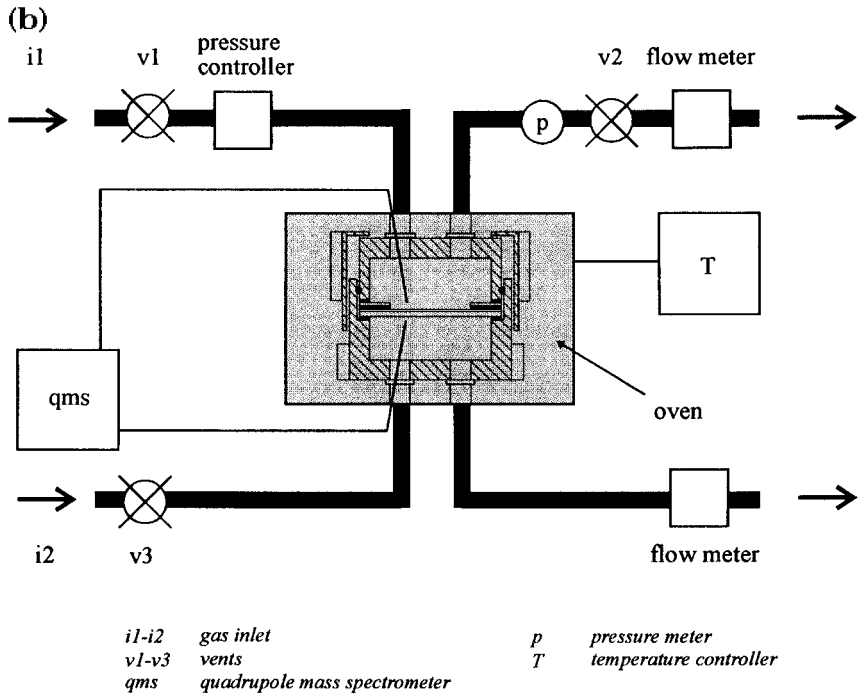

Figure 1. (a) Membrane reactor. (b) Experimental setup for gas separation studies.

tered zirconia thin films, which were made for comparison, showed that this loss of surface porosity seems to be not a process but a materials-specific effect. With about 105 $m^2\ g^{-1}$ the specific surface area of the sputtered ZrO_2-films is comparable to the e-beam evaporated YSZ thin films.

Supported Film Structure: Electron Beam Evaporation. Especially for gas-separation applications defect-free layers have to be produced in order to minimize nonspecific mass transport through cracks and pinholes. The preparation of dense, defect-free films with a thickness below 1 μm turned out to be a major problem. The reduction of membrane defect concentration became a major optimization parameter. Films with very high defect concentrations appear shadowed and stigmatized and could be sorted out directly. Good membrane quality was always associated with mirror-like properties. For better evaluation of defect concentrations gas permeation measurements were used. The results are given in terms of relative permeability P_{rel}, which is the ratio of permeating fluxes J/J_0 across the membrane with and without coating respectively. The permeating flux J is defined by

$$J = \frac{dV}{dt}\frac{1}{A\Delta p} \tag{2}$$

$$P_{rel} = \frac{J}{J_0} \times 100\% \tag{3}$$

where dV/dt is the volume flux, A is the active area of the membrane, and Δp is the pressure gradient across the membrane. Scanning electron microscopy was used for direct detection of microscopic cracks and provided the best insight into actual film structure, texture, thickness, density, porosity, uniformity, and interface quality.

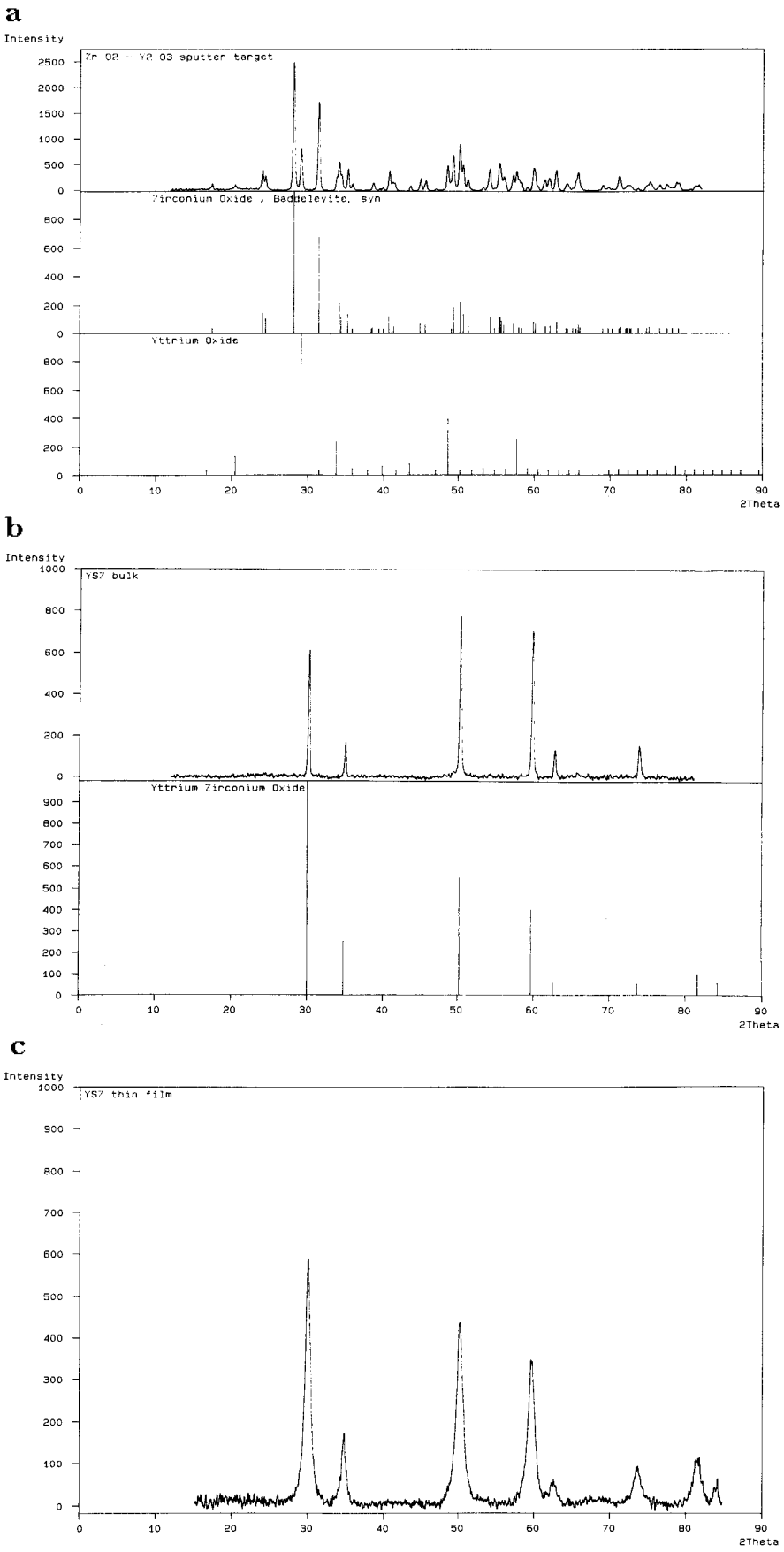

Figure 2. (a-c) Powder diffraction patterns of YSZ bulk and thin-film material.

In Figures 3a and b cross sections of zirconia thin films deposited by electron beam evaporation on an Anopore support membrane are shown. The lower part of both SEM micrographs indicates the parallel pore system of the support, in Figure 2b an additional layer of fine porous alumina (0.02 μm) can be identified. In both cases the coating can be seen as a defect-free layer on top of the surface without penetration of the pore

Table 2. Results of Nitrogen Adsorption Measurements on Thin-Film Materials[a]

sample	$A/m^2\ g^{-1}$	$V_{mp}/10^{-2}$ $cm^3\ g^{-1}$	r_{max}/nm	$d_{0.5}$/nm
YSZ (ev)	116−145	4.1−5.2	0.38−0.45	0.14−0.16
YSZ (sp)	105			
CSZ (ev)	108−109	3.8−3.9	0.37−0.49	0.15−0.20
YSZ-TiO_2 (ev)	69−73	2.4−2.6	0.76−0.90	0.26−0.30
YSZ-CeO_2 (ev)	92−97	3.3−3.5	0.50−0.59	0.13−0.14
LDC (ev)	58−60		(1−20)	
LDB (sp)	37			
Bi_2MoO_6 (sp)	6			
PbO-MgO (sp)	15			

[a] A, Dubinin surface area. V_{mp}, micropore volume. r_{max}, maximum in pore-size distribution. $d_{0.5}$, half-width of maximum in pore-size distribution. ev, thermally evaporated. sp, sputtered.

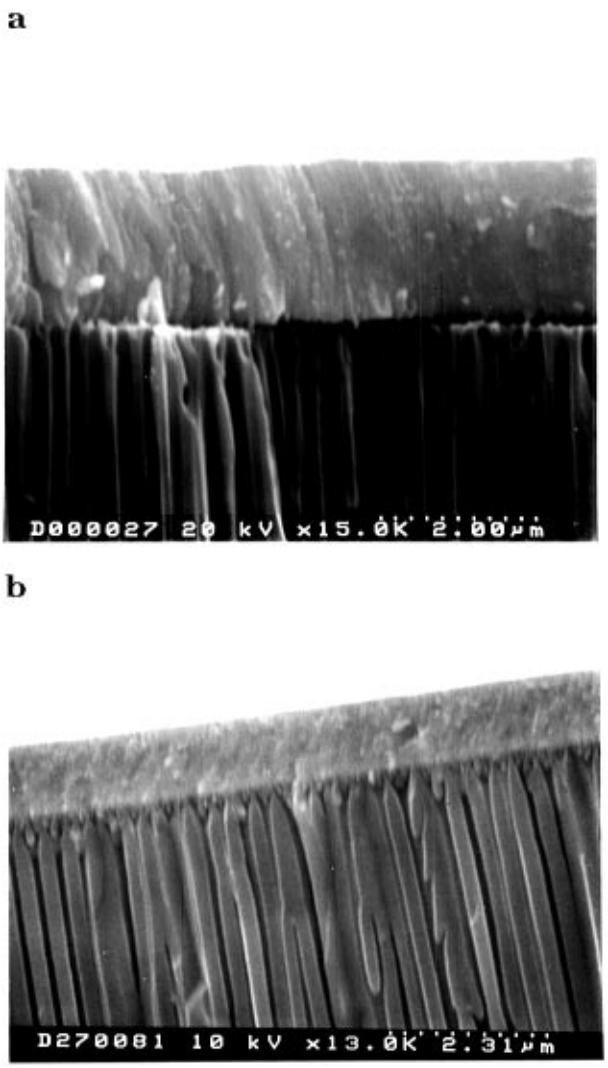

Figure 3. (a) YSZ-TiO_2 thin film on Anopore substrate with pore size 0.2 μm. (b) YSZ thin film on Anopore substrate with pore size 0.02 μm.

system of the support membrane, even for the relatively wide pore openings of 0.2 μm. This must be due to the formation of relatively large particles during film condensation.

Thorough pretreatment of the support membrane is required to minimize the defect concentration of the coating. The cleaning procedure consists of washing in hot acetone−pentane mixtures followed by ultrasonic treatment, calcination at 600 °C and glow discharge treatment in the vacuum chamber directly before film

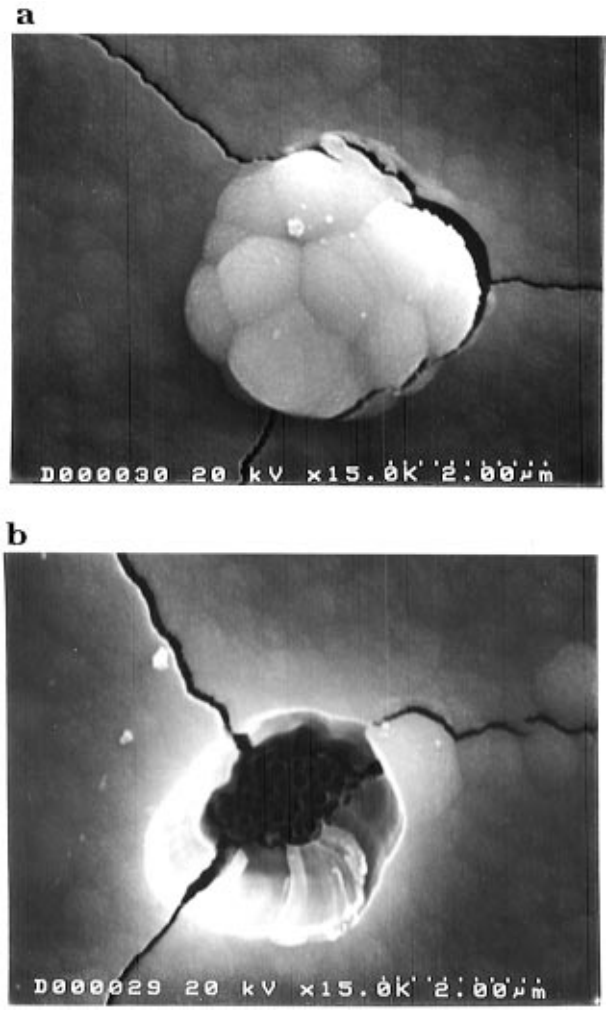

Figure 4. (a) Coating on contaminated surface viewed from top. (b) Same as in (a) with complete breakthrough of the coating down to support pore openings.

deposition. Each residual contaminant particle on the support surface results in the development of defects which also act as starting points for microscopic cracks (Figure 4).

SEM examinations at different stages of beginning film growth on Anopore substrates from reactive evaporation in 10^{-4} mbar of oxygen showed that continuous films begin to form at about 0.1 μm thickness. Below 0.1 μm thickness particles condense ringwise around the pore openings and grow by shadowing[28] of the original substrate surface structure. This mechanism is expected according to the zone-structure model by Thornton,[29] which proposes certain structural features of condensed films made by physical vapor deposition in dependence of partial pressure and T_s/T_m values, the ratio of substrate temperature and melting point of the condensate. Different structural zones 1, T, 2, and 3 with growing effective density are defined. All zirconia- and ceria-containing films prepared in this work are of zone-1 type where shadowing effects overcome the limited adatom surface diffusion. This results in domed tops with voided grain boundaries, to be seen on the surface in Figure 4. For very high melting materials

(28) Shadowing = geometric constraint imposed by roughness of the growing film and line-of-sight impingement of arriving atoms.

(29) Ohring, M. *The materials science of thin films*; Academic Press: San Diego, 1991.

such as zirconia, a high film density zone cannot be obtained below substrate temperatures of about 600 °C. These temperatures cannot be achieved with our equipment.

As a consequence the density of the thin-film materials is always reduced relative to the corresponding bulk systems. Combined gravimetric and SEM examinations showed that due to the porosity the stabilized zirconia thin films prepared in this work had an average density of about 4.3 g cm^{-3} which is 73% of the bulk density (YSZ-9: $\rho = 5.9$ g cm^{-3}). For this reason the oscillating quartz thickness monitor in the evaporation equipment has to be calibrated always. If bulk density is assumed for thickness monitoring, the measured thickness is much lower than the actual film thickness. SEM studies on membrane cross sections showed nearly no variation in film thickness across the support area. This may in part be due to the evaporation technique, where local differences are compensated directly during evaporation by substrate rotation. SEM micrographs of cross sections show intact coating edges and the membrane films do not show splintering upon breaking of the membrane, which points to a strong and solid interface bonding between coating and support.

Permeation measurements on membranes made by electron beam evaporation with a thickness of 0.3−0.5 μm proved this to be an ideal thickness range with optimum low permeability around 0.5−5% P_{rel} which indicates continuous films with low defect concentration. With growing film thickness the coating tends to crack. This effect could probably be due to intrinsic film tension when surpassing the critical film thickness above 0.5−1 μm.

Sol−Gel Modified Membranes. A repair of undesired porosity or too high defection concentration of membranes produced by electron beam evaporation was attempted by a sol−gel coating procedure with the aim of closing some residual microscopic cracks and pinholes. This was successfully achieved by the use of a zirconia sol−gel dipcoating procedure.[26] After drying and calcination at 300 °C the zirconia gel transforms to a totally amorphous glassy solid. Nitrogen adsorption measurements proved this to be purely microporous with pore radius 0.3 nm and a specific surface area of 140−170 m^2 g^{-1}.

SEM examinations showed that during dipcoating the solution tends to penetrate the support pore system completely, presumably because of strong capillary forces. So it can be assumed that small defects in the electrolyte film are filled with the zirconia sol and thus act like a repair kit for defective layers. It appeared that membranes prepared by e-beam evaporation tend to crack very readily upon calcination, if they are not dipcoated with a thin sol−gel layer.

If the coating−calcination cycle is repeated, an additional layer of microporous amorphous zirconia is deposited on top of the electrolyte film. It can serve as a protective coating for ultrathin films. An example for such a membrane is given in Figure 5.

To confirm that the sol−gel coating will have no influence on the final membrane performance, a control membrane was coated by the sol−gel method alone. In accordance with earlier results[25] multiple coatings were required for defect-free membranes. At least five coating−calcination cycles were necessary to obtain P_{rel} values below 5% which nearly seems to be the maximum performance of sol−gel coated membranes. Three coatings showed P_{rel} values around 10%, but the separation test failed, indicating still too many defects.

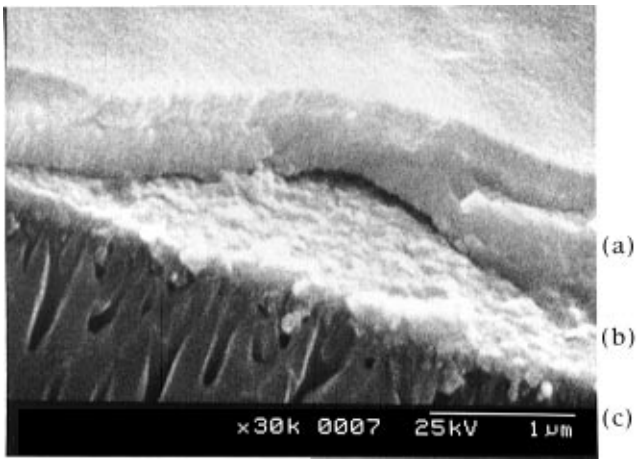

Figure 5. LDB electrolyte film (b) with 3-fold zirconia protective sol−gel coating (a) on Anopore 0.02 support membrane (c).

A single dipcoating treatment of 0.3−0.5 μm electrolyte membranes produced by electron beam evaporation results in a lowering of their relative permeabilities from 0.5−5.0% to 0.1−0.5%. This indicates successful filling of defects in the electrolyte layer by incorporated sol−gel material. For thin membranes a single sol−gel treatment proved sufficient to produce films of a quality sufficient for further investigations.

Supported Film Structure: rf Sputtering. Reactive rf sputtering was used for the preparation of YSZ, LDB, Bi_2MoO_6, and PbO−MgO films with 150−200 W rf power and a sputtering pressure of 5×10^{-3} mbar Ar/O_2. Coating rates were in the range 5−20 nm min^{-1}. With a maximum coating time of 30 min this results in a maximum film thickness of 0.15−0.6 μm.

Figure 6a shows a SEM micrograph of the cross section of a stabilized zirconia thin film deposited on Anopore support by rf sputtering. In contrast to stabilized zirconia membranes prepared by thermal evaporation, the sputtered film material tends to penetrate the supporting pore system. This is due to smaller film particle size during condensation of sputtered film material. In this case contaminated surfaces must not necessarily lead to defective coatings, as can be seen in Figure 6b. Shadowing effects are partially compensated by better distribution of film particles due to their smaller dimensions.

As a consequence of smaller particle size sputter coating results directly in dense, ultrathin films ($P_{rel} <$ 0.1%; $d < 0.6$ μm) without further need of modification. The lower melting point of bismuth and lead oxides leads to higher T_s/T_m values and therefore a higher density of the coating layers. Thornton zone structure model proposes zone-T-type layers, which are defined as fibrous grains with arrays of dense grain boundaries,[28] for the bismuth oxide already at room temperature. By raising the substrate temperature above 200 °C during deposition, we have obtained the zone-2-type region with columnar grains and dense grain boundaries. However, there was no apparent advantage in permeation properties over the T-type layer indicating no further improvement in film quality.

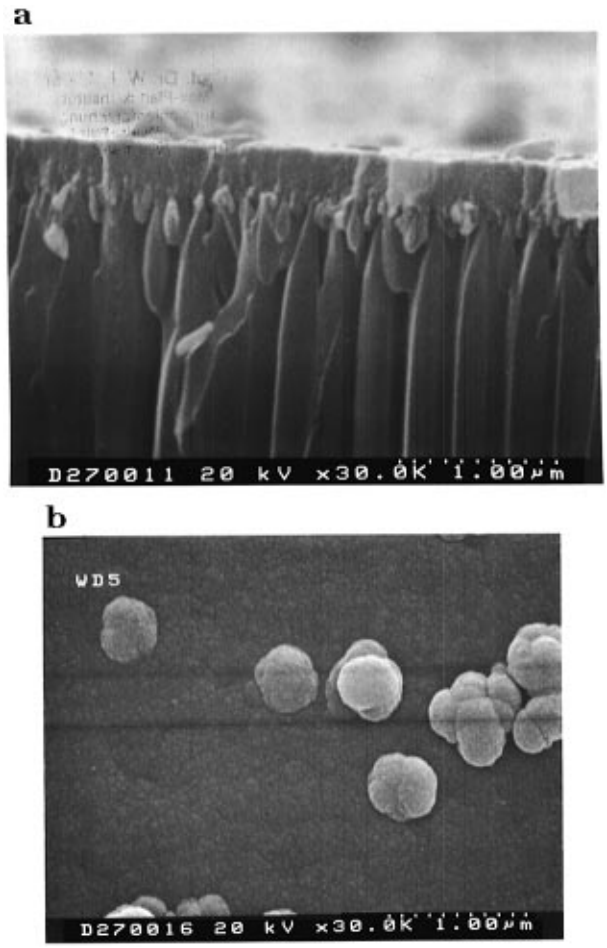

Figure 6. (a) Cross section of YSZ membrane prepared by rf sputtering on Anopore 0.02. (b) Same membrane as in Figure 6a, view from the top.

Gas Separation Measurements. Gas separation measurements were performed on several of the membranes and a mixture of He, Ar and O_2. The results are given in terms of the separation factor α, which for a gaseous mixture of components A and B ($M_A < M_B$) is defined by

$$\alpha(A/B) = (p_{A,P}/p_{B,P})(p_{B,R}/p_{A,R}) \quad (4)$$

where p is the partial pressure of each gas component, indexes R and P stand for retentate and permeate side of the membrane, respectively. If diffusion through small pores (pore diameter smaller than mean free path way of gas molecules) is controlling, the separation is limited by the theoretical Knudsen separation factor α:

$$\alpha_{Kn} = \sqrt{M_B/M_A} \quad (5)$$

where M denotes the molar mass of each component ($M_B > M_A$). As can be seen from eq 5, enrichment of lighter gas components normally indicates Knudsen diffusion mechanism. The gas separation factors of the membranes determined at ambient temperature and at the upper temperature limit of 300 °C of the membrane reactor are summarized in Table 3 (experimental error of separation factors ±0.01).

The zirconia-based electrolyte membranes 1−3 as well as the bismuth-based material 6 showed almost identical separation behavior. The P_{rel} were in the range 0.1−1% of the uncoated support membranes. The observed separation factors indicate pore diffusion transport by the Knudsen mechanism. Despite the low permeabilities and therefore low defect concentrations in these membranes, gas transport is still dominated by diffusion through the micropores of the electrolyte film material. The increase of inner surface does not measurably increase the ion conductivity at these low temperatures. High porosity at temperatures (here 300 °C) below effective solid-state ion transport acts as intrinsic defects of the coating layer.

The ceria containing electrolyte membranes 4−5 show poor separation properties as expected from the high defect concentrations indicated by relative permeabilities of 5−18%. The large mesopore content apparent in the pore size distribution of the LDC membranes is clearly the cause of this lack of separation.

The zirconia-based electrolyte 4 shows a broader micropore distribution tailing into the mesopore area, which seems to be caused by the ceria content.

Completely different results were obtained with the electrolyte membranes made from Bi_2MoO_6[19] and PbO−MgO,[22] respectively. The low intrinsic porosity of the materials results in relative permeabilities well below 0.1%. Although at ambient temperature pure Knudsen separation seems to dominate, at higher temperatures significant deviations were observed. At 300 °C the separation factor $\alpha(O_2/Ar)$ for both membranes exceeds the theoretical Knudsen limit. $\alpha(He/O_2)$ shows the corresponding decreasing value with increasing temperature, while with Knudsen diffusion a slight increase of α with temperature is expected. This indicates specific enrichment of oxygen by the membrane material.

The obtained oxygen selectivity for these two types of membranes could be due to ionic oxygen transport through the bulk layer of the electrolyte coating. This would support the concept of mixed conducting oxides as favorable membrane materials for oxygen selective membranes.[5] Impedance spectroscopic investigations, which were performed for Bi_2MoO_6,[30] proved this material to be a very good mixed conductor with good conductivity even at temperatures below 300 °C. We have observed a conductivity of 6.5×10^{-6} S/cm at 300 °C for our Bi_2MoO_6, 4 times as high as that of YSZ-9. The Arrhenius plot of the temperature dependence of the conductivity indicates that electronic conductance dominates below 300 °C (E_a = 8 kJ/mol) while above 300 °C the ionic conductivity dominates (E_a = 74 kJ/mol). The PbO−MgO materials also show conductivity already at temperatures as low as 350 °C (E_a = 74 kJ/mol).

Conclusions

By physical vapor deposition techniques it is possible to prepare membranes of various solid electrolytes of very low thickness (below 0.5 µm). In case of stabilized zirconia thermal evaporation leads to polycrystalline films with retained oxygen ion conducting crystal phase and composition and very large specific surface area due to microporosity. Although a large specific surface area of the film material is desirable for enhancing the oxygen exchange at the membrane surface, it is disfavorable as long as it controls the total transport.

(30) Ziehfreund, A. Dissertation Universität Essen, 1994.

Table 3. Results of Gas Separation Measurements on Various Solid Electrolyte Membranes[a]

no.	membrane	d/μm	A/m^2 g^{-1}	P_{rel}/m^2 g^{-1}	T/°C	$\alpha(O_2/Ar)$	$\alpha(He/O_2)$	$\alpha(He/Ar)$
1	YSZ (ev/sg)	0.3	115−145	0.1−0.08	25	1.04	1.45	1.50
					300	1.02	1.52	1.54
2	CSZ (ev/sg)	0.4	108−109	0.5−0.8	25	1.00	1.12	1.11
					300	1.01	1.16	1.17
3	YSZ-TiO_2 (ev/sg)	0.3	63−73	0.3−1.4	25	1.01	1.12	1.13
					300	1.01	1.20	1.21
4	YSZ-CeO2 (ev/sg)	0.5	92−97	6−18	25−300			
5	LDC (ev)	0.7	58−60	5−13	25−300			
6	LDB (sp)	0.6	37	0.3−0.1	25	1.06	1.12	1.19
					300	1.02	1.61	1.64
7	Bi_2MoO_6 (sp)	0.5	5.6	0.06−0.02	25	1.06	1.33	1.40
					300	1.18	1.26	1.49
8	PbO−MgO (sp)	0.4	14.7	0.07−0.03	25	1.01	1.18	1.19
					300	1.28	1.07	1.37
					α_{Kn}	1.12	2.83	3.16

[a] ev, evaporated. sg, sol-gel coating. sp, sputtered. α, α_{Kn} separation factor, Knudsen separation factor.

Clearly, porosity can only be beneficial to oxygen separation if its total contribution to permeability is low compared to the desired transport mechanism of ionic conductivity. Higher operating temperatures may help to compensate Knudsen pore diffusion by enhanced bulk ionic oxygen transport but are counterproductive with respect to the goal of low-temperature application.

Gas separation experiments performed with lead−magnesium oxide and bismuth molybdate membranes document that the materials described here have membrane properties. First results even indicate selective oxygen transport through the electrolyte layer at temperatures as low as 300 °C. We assume that we have seen a promising indication of ionic conduction, which has to be further examined. Bismuth molybdate with its mixed ionic and electronic conductivity properties, confirmed by impedance spectroscopy,[30] might be especially suited for such applications. Sputtering may be the preparation method of choice because of the direct formation of dense coatings and a rather low sensitivity to surface contaminations of the support membrane.

Acknowledgment. We thank H.-W. Schmidt for preparation of the reactor, Nissei Sangyo for access to their Hitachi scanning microscopes, and the BMFT (Grant 03C257B) for support.

CM9601953